Taylor & Francis
Taylor & Francis Group

Check for updates

In silico identification and validation of triarylchromones as potential inhibitor against main protease of severe acute respiratory syndrome coronavirus 2

Vaishali Chandel[a]*, Garima Tripathi[b]*, Seema A. Nayar[c,d], Brijesh Rathi[e], Abhijeet Kumar[f] and Dhruv Kumar[a]

[a]Amity Institute of Molecular Medicine and Stem Cell Research, Amity University Uttar Pradesh, Noida 201313, India; [b]Department of Chemistry, T. N. B. College, TMBU, Bhgalpur, Bihar, India; [c]Department of Microbiology, Government Medical College, Trivandrum, India; [d]Department of Microbiology, Sree Gokulam Medical College, Trivandrum, India; [e]Laboratory for Translational Chemistry and Drug Discovery, Department of Chemistry, Hansraj College, University of Delhi, New Delhi, India; [f]Department of Chemistry, Mahatma Gandhi Central University Motihari 845401, India

Communicated by Ramaswamy H. Sarma

ABSTRACT

The ongoing pandemic due to severe acute respiratory syndrome coronavirus 2 (SARS-CoV-2) caused COVID-19 has emerged as a severe threat to the life of human kind. The identification and designing of appropriate and reliable drug molecule for the treatment of COVID-19 patients is the pressing need of the present time. Among different drug targets, the main protease of SARS-CoV-2 is being considered as most effective target. In addition to the drug repurposing, different compounds of natural as well as synthetic origins are being investigated for their efficacy against different drug targets of SARS-CoV-2 virus. In that context, the chromone based natural flavonols have also exhibited significant antiviral properties against different targets of SARS-CoV-2. The in silico studies presented here discloses the efficacy of triarylchromones (TAC) as potential inhibitor against main protease of SARS-CoV-2. The molecular docking and ADMET study performed using 14 arylchromones which could easily be accessed through simple synthetic protocols, revealed best binding affinities in case of TAC-3 (–11.2 kcal/mol), TAC-4 (–10.5 kcal/mol), TAC-6 (–11.2 kcal/mol), TAC-7 (–10.0 kcal/mol). Additional validation studies including molecular dynamics simulation and binding energy calculation using MMGBSA for protein ligand complex for 100 ns revealed the best binding interaction of TAC-3, TAC-4, TAC-6, TAC-7 against main protease of SARS-CoV-2. Moreover, the in vitro and preclinical validation of identified compounds will help us to understand the molecular mechanisms of regulation of TACs against SARS-CoV-2.
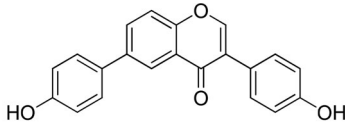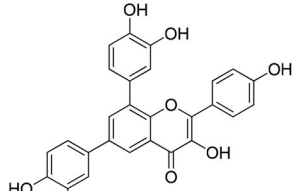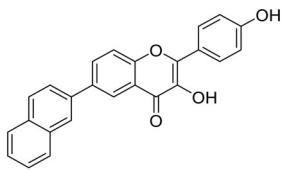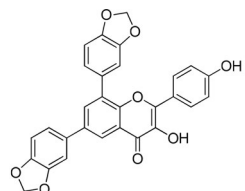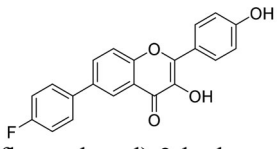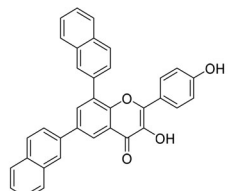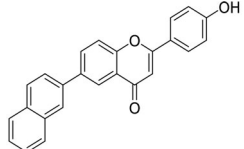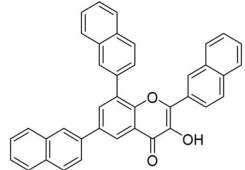
1. Introduction

The ongoing pandemic due to severe acute respiratory syndrome coronavirus 2 (SARS-CoV-2) has emerged as one the most contagious disease of last several decades (Rohit et al., 2020; Zheng, 2020; Zhu et al., 2020). Although various structural as well as biological aspects of this virus has already been explored but (Portelli et al., 2020; V'kovski et al., 2020) but several information regarding the specific drug targets, mechanism of action are yet to be established to discover an appropriate drug therapy. SARS-CoV-2 is an enveloped positive-sense RNA viruses, is one of the member viruses of Coronaviridae family and Coronavirinae subfamily (Astuti & Ysrafil, 2020; Yang et al., 2020). As per the current data provided by the World Health Organization (WHO), more than 54 millions confirmed cases and approx. 1.3 million deaths have been reported so far across the world since its first report from Wuhan in Dec. 2019, China and respiratory related infection and complications have emerged as one of the major cause of the death (Vincet & Taccone, 2020; http://
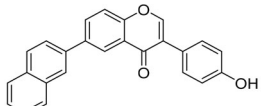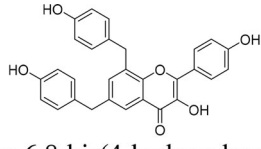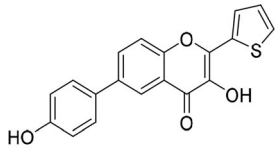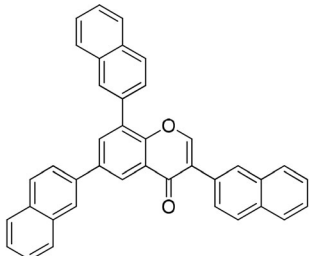
covid19who.int/). Apart from the lower respiratory tract infections, other organs such as kidney, liver, heart have also found to be greatly affected due to the infections due to SARS-CoV-2 virus (Gavriatopoulou et al., 2020; Huang et al., 2020). In order to trounce the existing health crisis, different strategies such as drug repurposing (Guy et al., 2020; Harrison, 2020; Serafin et al., 2020), discovery of new vaccines (Krammer, 2020; Tregoning et al., 2020; https://www.nature.com/articles/d41586-020-03248-7; https://www.pfizer.com/news.press-release/press-release-detail/pfizer-and-biontech-announce-vaccine-candidate-against) and convalescent plasma therapy (Focosi et al., 2020) are being employed. In that direction, immense efforts are also being made towards the discovery of effective therapeutic agents which could successfully bind with the different drug targets such as the spike (S) protein, enzymes such as proteases, viral RNA etc. and inhibit different steps of the infection (Akaji & Konno, 2020; Coelho et al., 2020; Preeti et al., 2020; Rane et al., 2020; Zhao et al., 2021; Zhu et al., 2020). For examples the spike (S) protein of SARS-CoV-2 interacts with different receptors such as

CONTACT Dhruv Kumar ✉ dkumar13@amity.edu, dhruvbhu@gmail.com ● Amity Institute of Molecular Medicine and Stem Cell Research, Amity University, Uttar Pradesh, Noida 201313, India; Abhijeet Kumar ✉ abhijeetkumar@mgcub.ac.in ● Department of Chemistry, Mahatma Gandhi Central University, Motihari 845401, India
*Vaishali Chandel and Garima Tripathi are equal contribution.
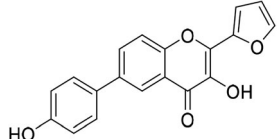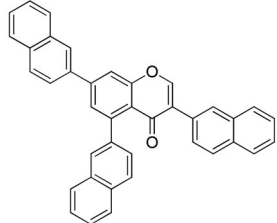
Table 1. List of arylchromones as potential drug candidate against main protease of SARS-CoV-2

S. no.	Diarylchromone (DAC)	S. no.	Triarylchromone (TAC)
1.	3,6-bis(4-hydroxyphenyl)-4*H*-chromen-4-one **(DAC-1)**	8.	6,8-bis(3,4-dihydroxyphenyl)-3-hydroxy-2-(4-hydroxyphenyl)-4*H*-chromen-4-one **(TAC-1)**
2.	3-hydroxy-2-(4-hydroxyphenyl)-6-(naphthalen-2-yl)-4*H*-chromen-4-one **(DAC-2)**	9.	6,8-bis(benzo[*d*][1,3]dioxol-5-yl)-3-hydroxy-2-(4-hydroxyphenyl)-4*H*-chromen-4-one **(TAC-2)**
3.	6-(4-fluorophenyl)-3-hydroxy-2-(4-hydroxyphenyl)-4*H*-chromen-4-one **(DAC-3)**	10.	3-hydroxy-2-(4-hydroxyphenyl)-6,8-di(naphthalen-2-yl)-4*H*-chromen-4-one **(TAC-3)**
4.	2-(4-hydroxyphenyl)-6-(naphthalen-2-yl)-4*H*-chromen-4-one **(DAC-4)**	11.	3-hydroxy-2,6,8-tri(naphthalen-2-yl)-4*H*-chromen-4-one **(TAC-4)**
5.	3-(4-hydroxyphenyl)-6-(naphthalen-2-yl)-4*H*-chromen-4-one **(DAC-5)**	12.	3-hydroxy-6,8-bis(4-hydroxybenzyl)-2-(4-hydroxyphenyl)-4*H*-chromen-4-one **(TAC-5)**
6.	3-hydroxy-6-(4-hydroxyphenyl)-2-(thiophen-2-yl)-4*H*-chromen-4-one **(DAC-6)**	13.	3,6,8-tri(naphthalen-2-yl)-4*H*-chromen-4-one **(TAC-6)**

Table1. Continued.

S. no.	Diarylchromone (DAC)	S. no.	Triarylchromone (TAC)
7.	2-(furan-2-yl)-3-hydroxy-6-(4-hydroxyphenyl)-4H-chromen-4-one (**DAC-7**)	14.	3,5,7-tri(naphthalen-2-yl)-4*H*-chromen-4-one (**TAC-7**)

Figure 1. (A) Main protease (PDB ID-6LU7) of SARS-CoV-2. The structure is shown in ribbon representation, coloured from the N-terminus to the C-terminus with colours changing from RED (interacting chain A) to blue (interacting chain B). (B) Surface representation structure of Main protease (PDB ID-6LU7) of SARS-CoV-2.
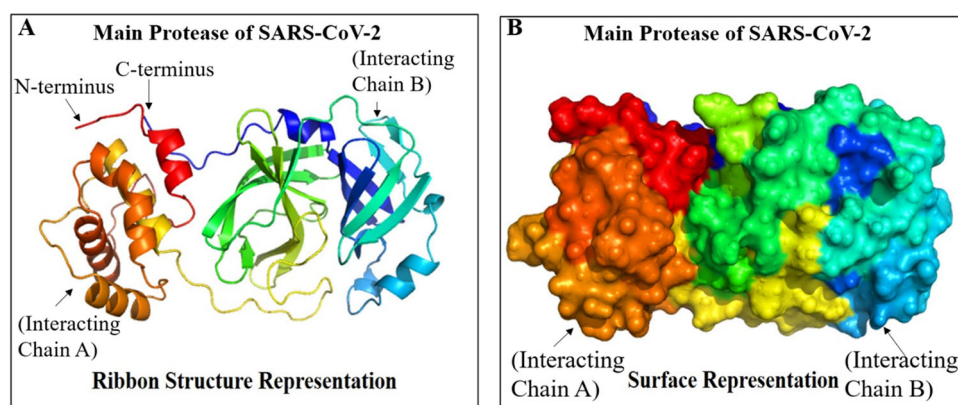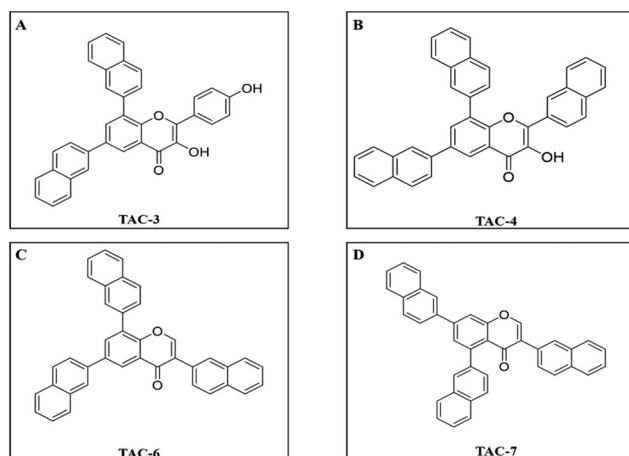

Figure 2. The 2D structure of A. TAC-3, B. TAC-4, C. TAC-6, and D. TAC-7. (TAC: triarylchromones).

Table 2. Molecular docking analysis of arylchromones against major protease (6LU7) of SARS-CoV-2.

S. no.	Arylchromones	Binding affinity (kcal/mol)
1.	DAC-1	−8.2
2.	DAC-2	−8.8
3.	DAC-3	−6.6
4.	DAC-4	−8.4
5.	DAC-5	−8.0
6.	DAC-6	−7.7
7.	DAC-7	−6.8
8.	TAC-1	−8.9
9.	TAC-2	−8.5
10.	TAC-3	−11.2
11.	TAC-4	−10.5
12.	TAC-5	−8.7
13.	TAC-6	−11.2
14.	TAC-7	−10.0

angiotensin-converting enzyme 2 (ACE-2), TM protease serine 2 (TMPRSS-2) etc. present on the host cell and facilitates the viral entry (Ali & Vijayan, 2020; Huang et al., 2020). Similarly, proteases such as Mpro or 3CL-protease are also being explored as excellent drug targets due to their involvement in enhancing viral loads and the growth of virus (Wu et al., 2020; Zhang et al., 2020). Despite of the growing understanding about the potential drug targets and fast-track research towards the development of the therapeutic agent, the discovery of appropriate and widely applicable drug therapy is still awaited. Some of the vaccines such as mRNA-1273 and BNT162b2 have

exhibited promising results so far (Jackson et al., 2020; Walsh et al., 2020). Except m-RNA based some of these vaccine candidates, no other effective and robust drug therapy could be discovered. Since the surfacing of the first case in China, the efficacy of several natural products as well as FDA-approved drugs of diverse verities has rigorously been investigated. For example, the effectiveness of drugs such as chloroquines, lopinavir, remdisivir, dexamethasone, ivermectin etc. have been investigated so far against COVID-19 but none of these could be established as an effective drug against SARS-CoV-2 (Cao & Yang, 2020; Chaccour et al., 2020; Ferner & Aronson, 2020; Lammers et al., 2020; Wang et al., 2020). Similarly, the efficacy of natural products and phytochemicals against COVID-19 and other viruses has also been explored (Aucoin & Cooley, 2020;

Table 3. ADME properties of selected COVID-19 main protease (6LU7) inhibitors.

| S. no. | Compound/ligand | ADME properties Lipinki's rule or rule of five (ROF) | | Drug likeliness |
		Properties	Values	
1.	DAC-1	Molecular weight (<500 Da)	330.33	Yes
		Log P (<5)	3.61	
		H-bond donar (5)	2	
		H-bond acceptor (<10)	4	
		ROF score	0	
2.	DAC-2	Molecular weight (<500 Da)	380.39	Yes
		Log P (<5)	4.58	
		H-bond donar (5)	2	
		H-bond acceptor (<10)	4	
		ROF score	0	
3.	DAC-3	Molecular weight (<500 Da)	348.32	Yes
		Log P (<5)	4.0	
		H-bond donar (5)	2	
		H-bond acceptor (<10)	5	
		ROF score	0	
4.	DAC-4	Molecular weight (<500 Da)	364.39	Yes
		Log P (<5)	5.00	
		H-bond donar (5)	1	
		H-bond acceptor (<10)	3	
		ROF score	0	
5.	DAC-5	Molecular weight (<500 Da)	364.39	Yes
		Log P (<5)	4.91	
		H-bond donar (5)	1	
		H-bond acceptor (<10)	3	
		ROF score	0	
6.	DAC-6	Molecular weight (<500 Da)	336.36	Yes
		Log P (<5)	3.69	
		H-bond donar (5)	2	
		H-bond acceptor (<10)	4	
		ROF score	0	
7.	DAC-7	Molecular weight (<500 Da)	320.30	Yes
		LogP (<5)	3.02	
		H-bond donar (5)	2	
		H-bond acceptor (<10)	5	
		ROF score	0	
8.	TAC-1	Molecular weight (<500 Da)	470.43	Yes
		Log P (<5)	3.46	
		H-bond donar (5)	6	
		H-bond acceptor (<10)	8	
		ROF score	1	
9.	TAC-2	Molecular weight (<500 Da)	494.45	Yes
		Log P (<5)	4.63	
		H-bond donar (5)	2	
		H-bond acceptor (<10)	8	
		ROF score	0	
10.	TAC-3	Molecular weight (<500 Da)	506.55	No
		Log P (<5)	6.71	
		H-bond donar (5)	2	
		H-bond acceptor (<10)	4	
		ROF score	2	
11.	TAC-4	Molecular weight (<500 Da)	540.61	No
		Log P (<5)	7.99	
		H-bond donar (5)	1	
		H-bond acceptor (<10)	3	
		ROF score	2	
12.	TAC-5	Molecular weight (<500 Da)	466.48	Yes
		Log P (<5)	4.59	
		H-bond donar (5)	4	
		H-bond acceptor (<10)	6	
		ROF score	0	
13.	TAC-6	Molecular weight (<500 Da)	524.61	No
		Log P (<5)	8.38	
		H-bond donar (5)	0	
		H-bond acceptor (<10)	2	
		ROF score	2	
14.	TAC-7	Molecular weight (<500 Da)	524.61	No
		Log P (<5)	8.38	
		H-bond donar (5)	0	
		H-bond acceptor (<10)	2	
		ROF score	2	
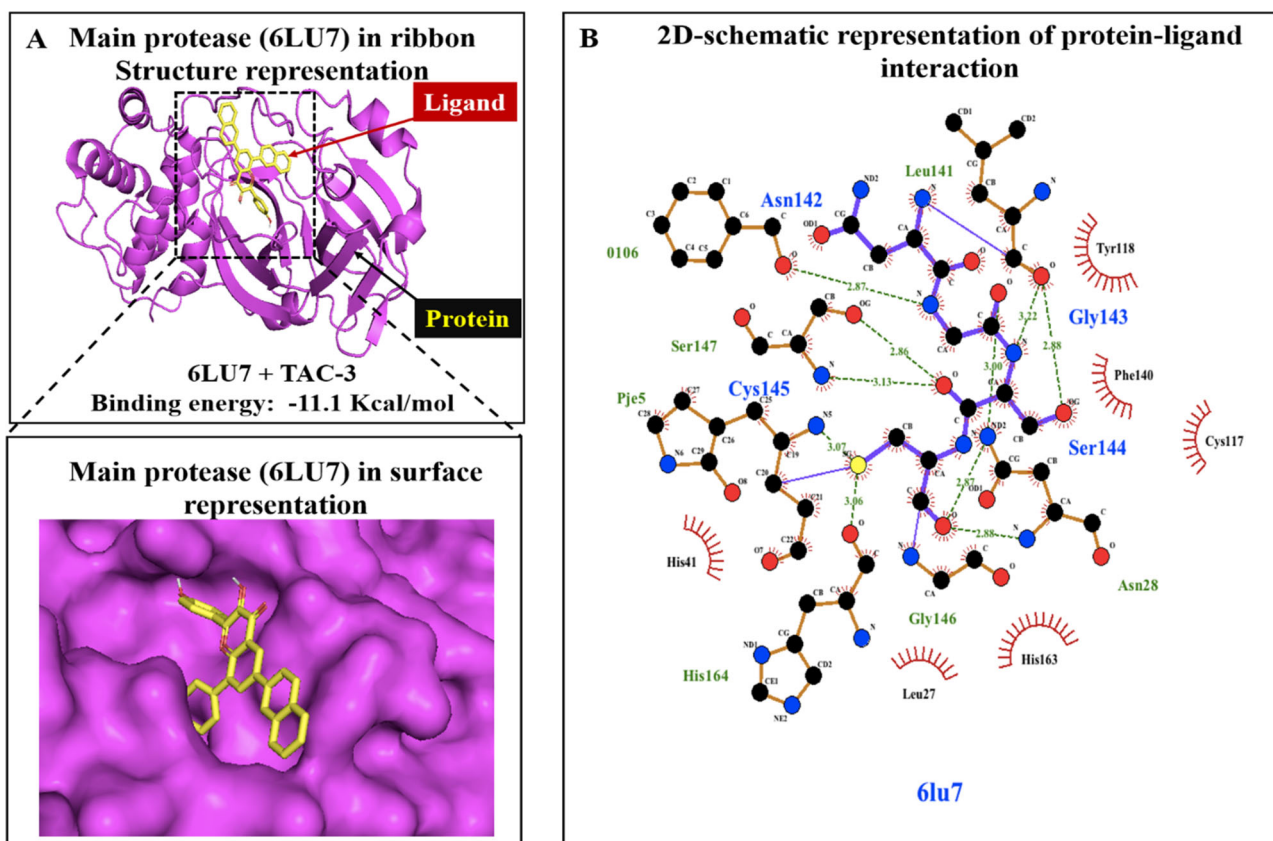
Figure 3. Docking analysis and visualisation of protein–ligand complex (A) Molecular docking analysis between main protease (PDB ID-6LU7) of SARS-CoV-2 and TAC-3. The protein 6LU7 is represented in 3D ribbon structure (pink) and the ligand is represented in yellow colour. The zoom in figure represents surface representation between the active site of the protein and ligand. (B) 2D schematic representation of protein–ligand interaction by LIGPLOT. Hydrogen bonds are indicated using dashed lines between the atoms involved in the interaction. Hydrophobic contacts are represented using red arc with spokes radiating towards the ligand atom in contact.

Kumar et al., 2020; Straughn & Kakar, 2020; Verma et al., 2020). In particular, the therapeutic values of chromone as core scaffolds are well established in the literature (Gaspar et al., 2014; Keri et al., 2014). Interestingly chromone scaffold containing phytochemicals such as quercetin, fisetin, etc. which are part of our dietary supplements, have also exhibited their efficacy against different drug targets of SARS-CoV-2 (Derosa et al., 2020; Seri et al., 2020).

In view of the immense therapeutic importance of these chromone containing heterocycles, especially as anti-viral agent, we envisaged that such therapeutic activity could be enhanced by functionalizing the chromone scaffold with appropriate functional groups and moieties. Flavoxate, Pranlukast, Disodium cromoglycate (DSCG) etc. are examples of synthetically produced drugs with chromone scaffold which have displayed excellent efficacy in the treatment of urinary and asthmatic disorders respectively (Gaspar et al., 2014; Reis et al., 2017). Therefore, the aim of the present *in silico* study was to investigate the efficacy of newly designed *di-* and *triaryl chromones* (Table 1) which could easily be accessed following literature known reaction protocols such as metal-catalyzed cross-coupling and C–H activation reactions (Choi et al., 2016; Kim et al., 2012; Rao & Kumar, 2014), against the SARS-CoV-2 main protease (6LU7) as potential drug target. 6LU7 is the major protease is the major protein in SARS-CoV-2 that has been structured and repositioned in the PDB database recently and is widely accessible around the globe. As shown in Figure 1A, it

represents the ribbon structure representation and (B) surface representation of COVID-19 main protease (6LU7) with interacting chain A and B. It is important to underline that compared to the natural product; the synthetic analogues allow the large scale synthesis in relatively short span of time. In addition to that, the pharmacological activities of these could easily be modulated through modification in the substituent.

2. Materials and methods

The SARS-CoV-2 virus main protease (PDB ID- 6LU7) structure was obtained from the RCSB PDB (protein data bank) database (http://www.rcsb.org). Prior to docking or analysis, the solvation parameters, charge assignment, and fragmental volumes to the SARS-CoV-2 main protease was done using the Autodock Tool 4 (ADT) (Morris et al., 2009; Sumit et al., 2020; Vivek et al., 2020). Further optimization of the protein molecule was done using Autodock Tool for the molecular docking (Chandel et al., 2020).

2.1. Ligand preparation

The selected compounds in 3D SDF format were screened in order to select the best hits. The 2D ligand structures were designed using Chemsketch program (Figure 2; Table 2). Avogadro program was used to optimize the ligands. Open
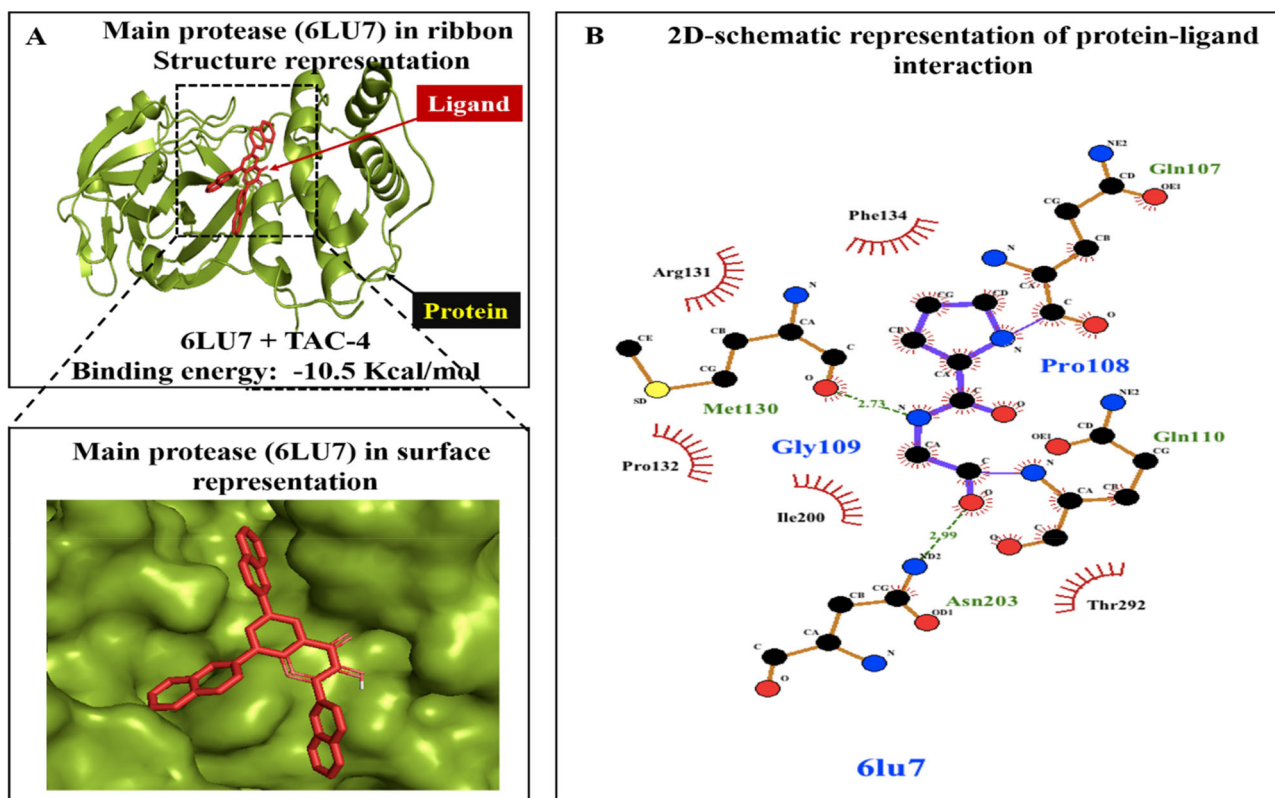
Figure 4. Docking analysis and visualisation of protein–ligand complex (A) Molecular docking analysis between Main protease (PDB ID-6LU7) of SARS-CoV-2 and TAC-4. The protein 6LU7 is represented in 3D ribbon structure (green) and the ligand is represented in orange colour. The zoom in figure represents surface representation between the active site of the protein and ligand. (B) 2D schematic representation of protein–ligand interaction by LIGPLOT. Hydrogen bonds are indicated using dashed lines between the atoms involved in the interaction. Hydrophobic contacts are represented using red arc with spokes radiating towards the ligand atom in contact.

Babel was used to convert the ligands into the PDB format. The ligands were first optimized and converted to PDBQT format in order to further simplify the process using the PyRx virtual screening tool-python prescription 0.8.

2.2. Compound screening using PyRx program

PyRx software was used for the purpose of molecular screening of all the library of compounds by autodock wizard as the engine for molecular docking (Morris et al., 2008). The ligands were considered to be flexible during the docking period and the protein was considered to be rigid. Auto Grid engine in PyRx was used for the generation of configuration file for the grid parameters. The PyRx application was also used to predict/understand the amino acids residues present in the active site of the protein that interact with the ligands. The results less than 1.0A° in positional root-mean-square deviation (RMSD) were clustered together and considered ideal for identifying the favourable binding. The most negative (highest binding energy) was considered as the best candidate with maximum binding energy (Chandel et al., 2020; Rashmi et al., 2020).

2.3. Analysis and visualization

Pymol version 2.3.4 was used for the visual analysis of the docking site and the validation of results were done using Autodock-Vina (Rauf et al., 2015).

2.4. ADME analysis

The ADME properties (absorption, distribution, metabolism, excretion, and toxicity) of the selected compound were calculated using online Swiss ADME program (Diana et al., 2007). The major parameters for ADMET associated properties includes Lipinski's rule of five (H bond acceptor, H bond donor, molecular weight, water/octanol partition coefficient), pharmacokinetic properties, the solubility of the drug, and drug likeliness were considered. The values of the observe properties are presented in Table 3.

2.5. Molecular dynamics (MD) and molecular simulation (MS) study

Selected complexes were prepared prior to MD simulation in the protein preparation wizard and Prime module of Schrödinger suite (Chandel et al., 2020; Schröndinger, 2020; Schrondinger, 2016; Schrondinger, 2020-1). Removal of steric clashes and strained bonds/angles were done by performing a restrained energy minimization, allowing movement in heavy atoms up to 0.3 Å. Extensive 100 ns MD simulation was carried out for both complexes through Desmond (D. E. Shaw Research, New York, NY, 2015) to access the binding stability of compounds with their respective protein complex. The standard fixed-charged force fields were used to optimize the complex. These complexes were solvated in TIP3P water model and 0.15 M NaCl to mimic a physiological ionic
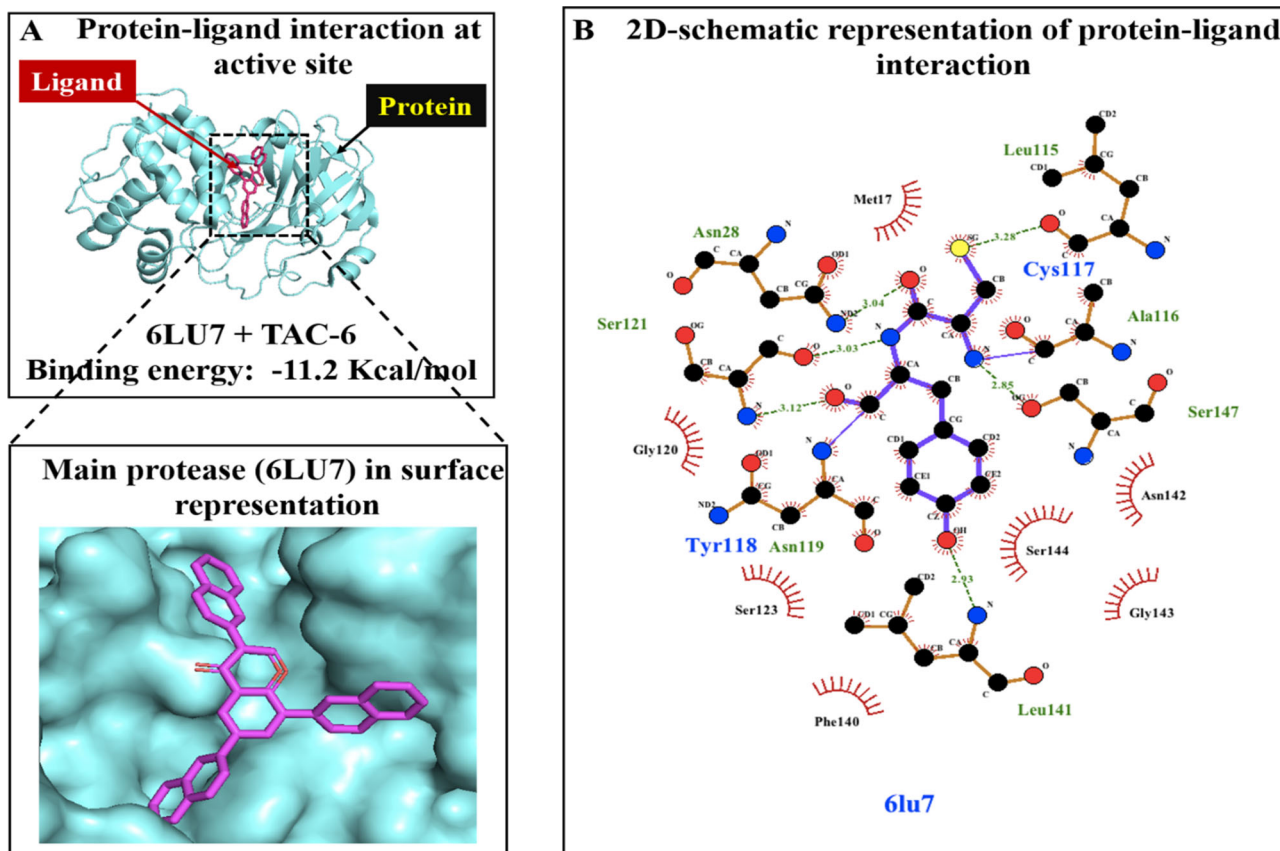
Figure 5. Docking analysis and visualisation of protein–ligand complex (A) Molecular docking analysis between Main protease (PDB ID-6LU7) of SARS-CoV-2 and TAC-6. The protein 6LU7 is represented in 3D ribbon structure (black) and the ligand is represented in light brown colour. The zoom in figure represents surface representation between the active site of the protein and ligand. (B) 2D schematic representation of protein–ligand interaction by LIGPLOT. Hydrogen bonds are indicated using dashed lines between the atoms involved in the interaction. Hydrophobic contacts are represented using red arc with spokes radiating towards the ligand atom in contact.
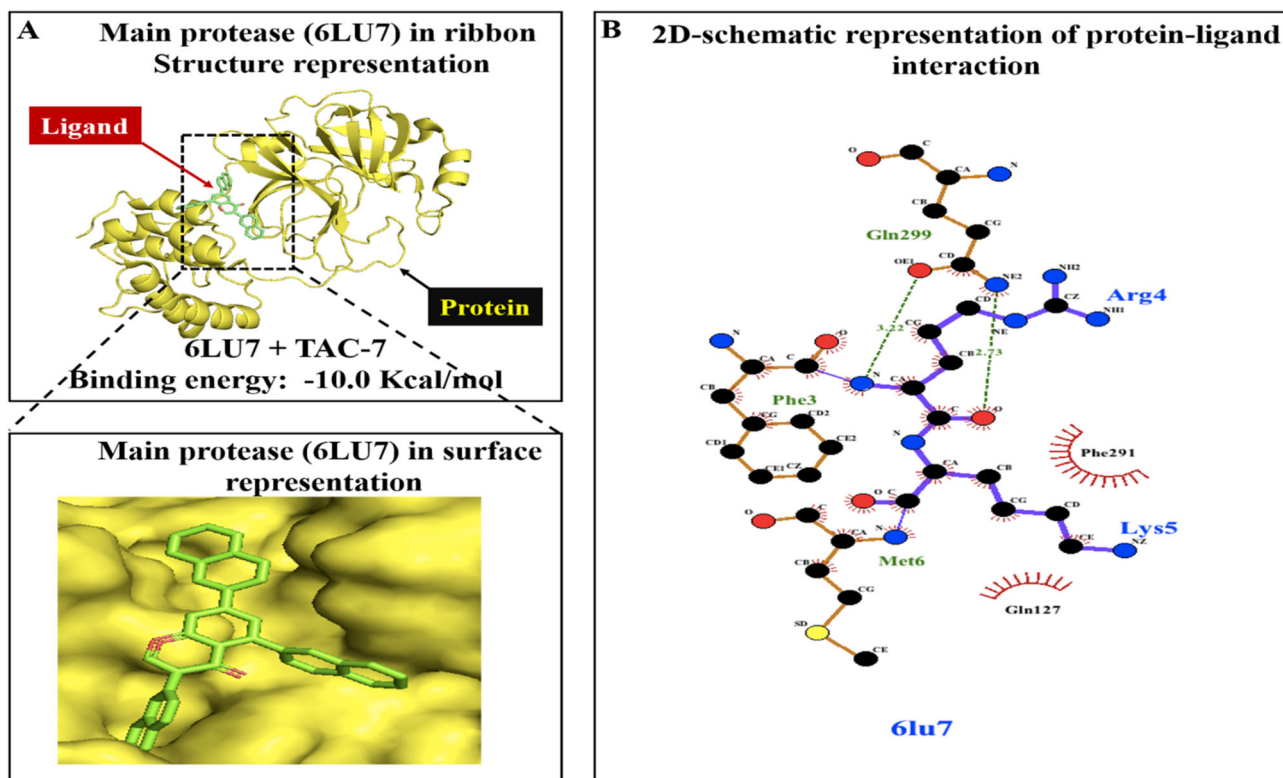
Figure 6. Docking analysis and visualisation of protein–ligand complex (A) Molecular docking analysis between Main protease (PDB ID-6LU7) of SARS-CoV-2 and TAC-7. The protein 6LU7 is represented in 3D ribbon structure (orange) and the ligand is represented in blue. The zoom in figure represents surface representation between the active site of the protein and ligand. (B) 2D schematic representation of protein–ligand interaction by LIGPLOT. Hydrogen bonds are indicated using dashed lines between the atoms involved in the interaction. Hydrophobic contacts are represented using red arc with spokes radiating towards the ligand atom in contact.
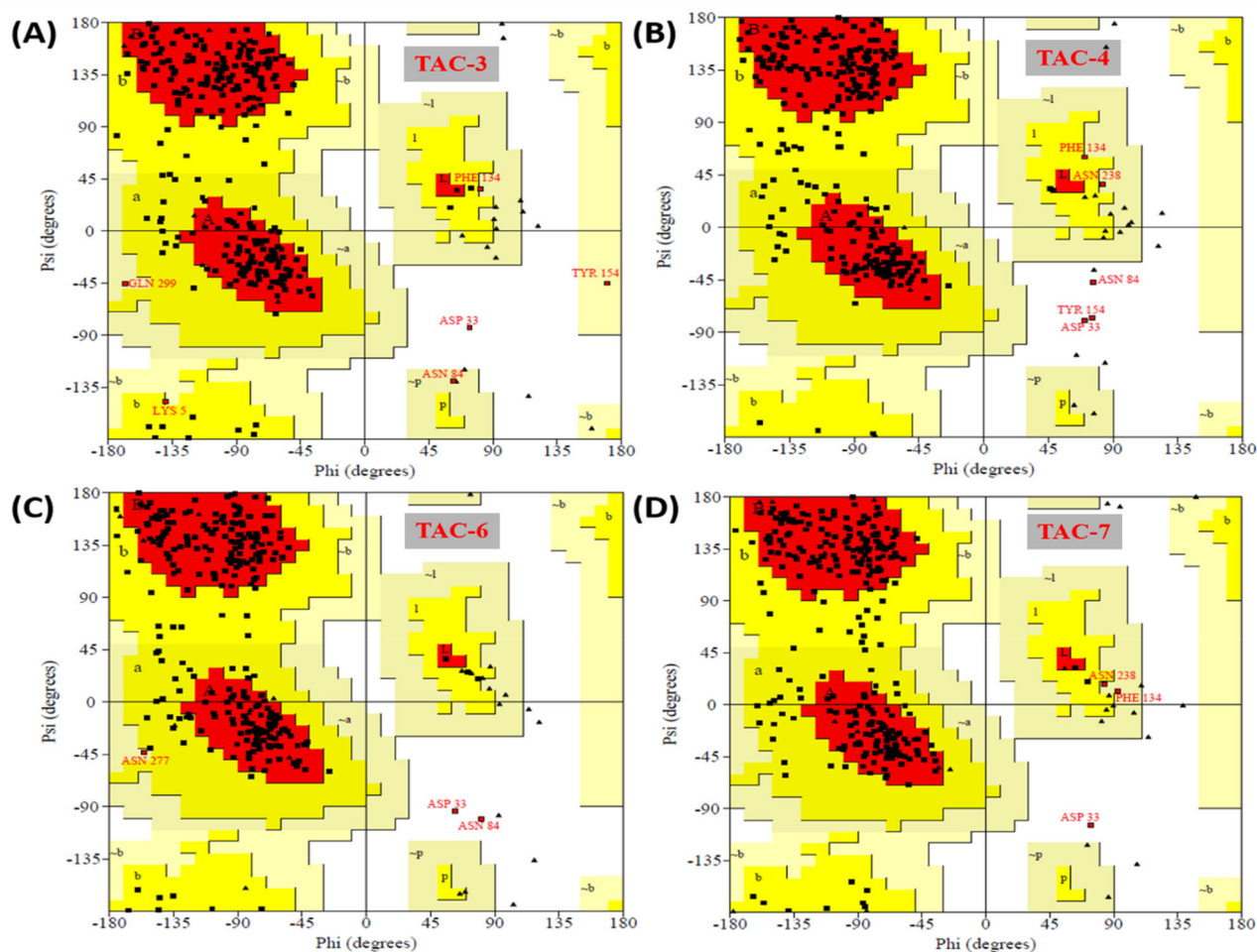
Figure 7. Ramachandran plot: (A) complex TAC-3, (B) complex TAC-4, (C) complex TAC-6, and (D) complex TAC-7. The red region in the plot indicates the favoured region, light yellow coloured region indicates generously slowed region, yellow region indicates allowed region and white region indicates disallowed regions. Torsion angle is determined by the Phi and Psi angles. Maximum points are within the most favoured regions.

Table 4. Occurrence of residues in favoured, additional-allowed, generously-allowed, and disallowed region.

Region	Complex TAC-3	Complex TAC-4	Complex TAC-6	Complex TAC-7
No. of residues lie in favoured region	217 (81.9%)	217 (81.9%)	214 (80.8%)	209 (78.9%)
No. of residues lie in additional allowed region	42 (15.8%)	43 (16.2%)	48 (18.1%)	53 (20.0%)
No. of residues lie in generously allowed region	5 (1.9%)	2 (0.8%)	1 (0.4%)	2 (0.8%)
No. of outlier residues	1 (0.4%)	3 (1.1%)	2 (0.8%)	1 (0.4%)

Table 5. Binding free energy calculation by MMGBSA

Entry	Complex	ΔG docked complex	ΔG after MD simulation
1	Complex TAC-3	−78.36	−97.93
2	Complex TAC-4	−66.89	−51.19
3	Complex TAC-6	−64.75	−78.44
4	Complex TAC-7	−57.52	−89.74

concentration. The full system energy minimization step was done for 100ps.

The MD simulation was run at constant 300 K temperature, standard pressure (1.01325 bar), within an orthorhombic box with buffer dimensions $10 \times 10 \times 10$ Å^3 and NPT ensemble. The energy (kcal/mol) was recorded at interval of 1.2 ps. The protein–ligand complex system was neutralized by balancing the net charge of the system by adding Na$^+$ or Cl$^-$ counter ions. The Nose–Hoover chain and Martyna–Tobias–Klein dynamic algorithm was used maintain the temperature of all the systems at 300 K and pressure 1.01325 bar, respectively.

3. Results and discussion

The arylchromones (1–14, Table 1) selected for our purposes could easily be prepared using literature known synthetic protocols mainly under the metal-catalyzed cross-coupling reaction protocols.

The potential drug likeness and efficacy of these functionalized chromones were investigated using *in silico* studies including molecular docking, ADME analysis and molecular dynamics simulation studies which have separately been described in the following sections. Molecular docking study reveals the strength and binding energy of a specific ligand by which a compound interacts with and binds to the active site pocket of a target protein. A compound with lesser binding energy is considered as a possible drug candidate. In order to understand the possible effect of the compounds against main protease 6LU7, molecular docking study of 14 active compounds was performed (Table 2). Docking results
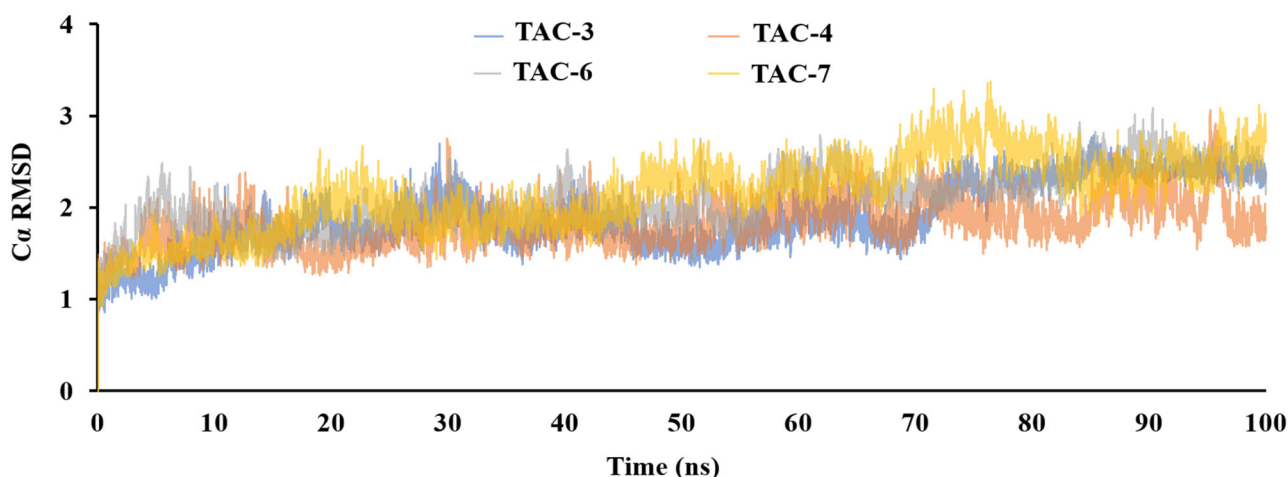
Figure 8. Cα RMSD Plot of complex TAC-3, 4, 6 and 7. Root mean square deviation (RMSD) was carried out for the MD simulation of each system.
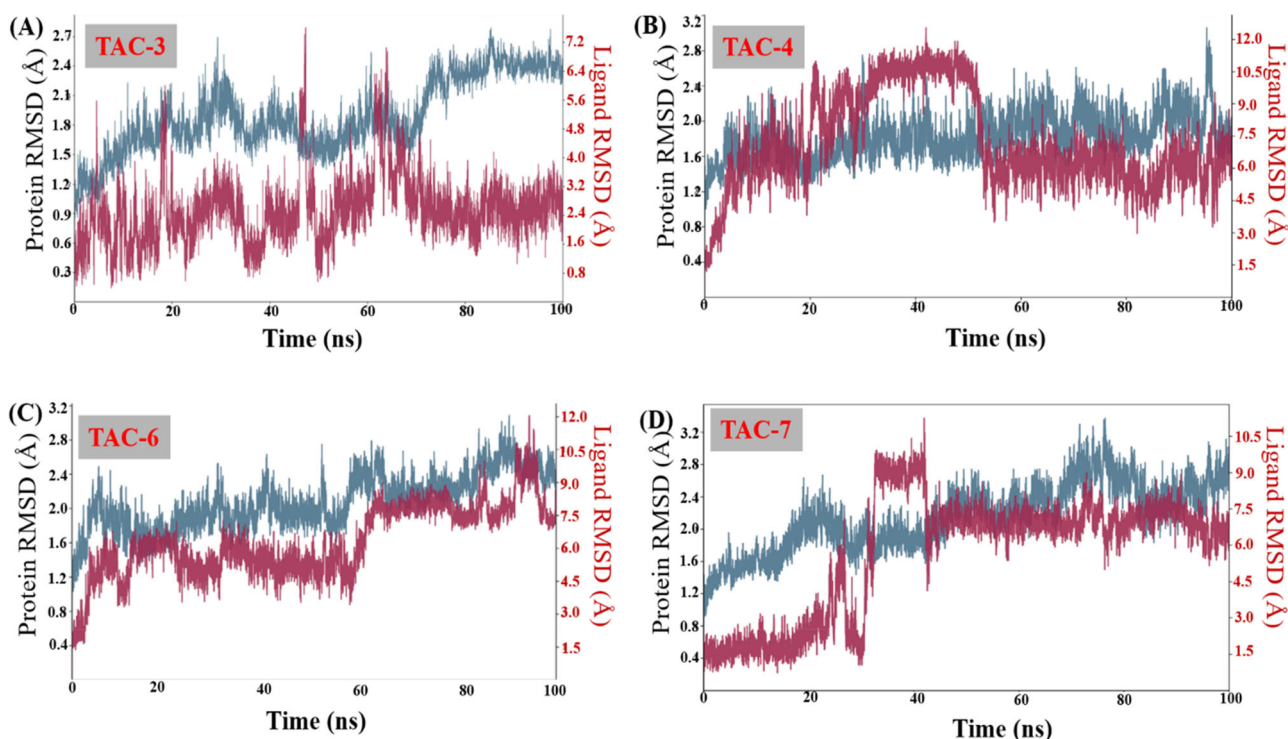

Figure 9. Protein–ligand RMSD plot: (A) complex TAC-3, (B) complexTAC-4, (C) complex TAC-6, and (D) complexTAC-7. Root mean square deviation (RMSD) plots of the protein–ligand complexes against the simulation time of 100 ns. The ligand TAC-3, TAC-4, TAC-6 and TAC-6 are shown in the red colour and the protein main protease (6LU7) side chain is shown in the blue colour.

of main protease 6LU7 with selected 4 compounds (TAC-3, TAC-4, TAC-6, TAC-7) revealed favourable binding energy and were observed to be as the best molecules at the major target site of the protein. The chemical structure of the selected 4 active compounds is shown in Figure 2. The molecular docking study and visualisation of main protease 6LU7 binding TAC-3, TAC-4, TAC-6, and TAC-7 are shown in Figures 3–6, respectively.

Out of the four compounds, *TAC-6* exhibited the best docking score (binding energy) i.e. −11.2 Kcal/mol with SARS-CoV-2 Main Protease 6LU7. The 2D schematic representation of protein-ligand interaction is represented by LIGPLOT representing the major amino acid residues of compound 13 binding on the active site pocket of the protein 6LU7 (Figure 5). TAC-*3* exhibited (−11.1 kcal/mol) binding

energy with main protease 6LU7. TYR118, HIS41, LEU27, HIS163, CYS117, PHE140 are the amino acid residues participating in the interaction at the binding pocket of COVID-19 (Figure 3). The 2D schematic representation of protein–ligand interaction is represented by LIGPLOT representing the major amino acid residues of TAC-3 binding on the active site pocket of the protein 6LU7. TAC-4 exhibited (−10.5 kcal/mol) binding energy with main protease 6LU7. ARG131, PHE134, THR292, ILE200, and PRO132 are the amino acid residues participating in the interaction at the binding pocket of COVID-19 (Figure 4). The 2D schematic representation of protein–ligand interaction is represented by LIGPLOT representing the major amino acid residues of compound 10 binding on the active site pocket of the protein 6LU7. TAC-7
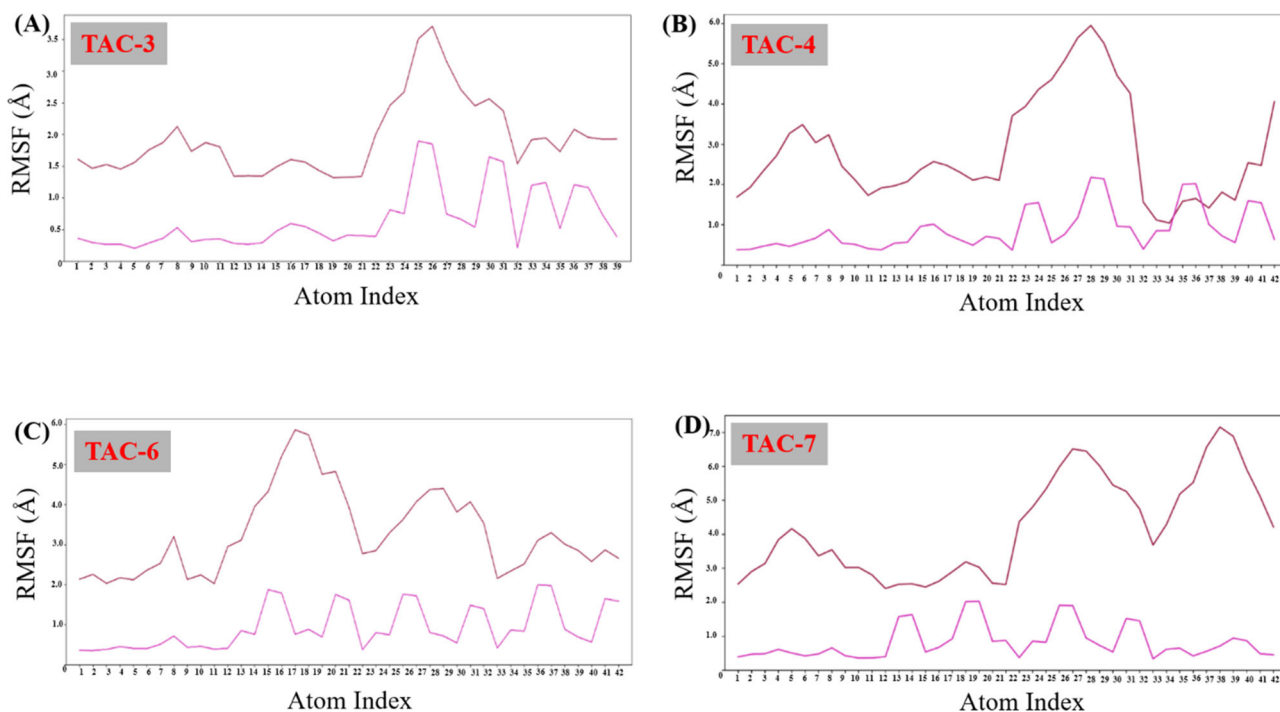
Figure 10. Ligand RMSF: (A) complex TAC-3, (B) complexTAC-4, (C) complex TAC-6, and (D) complexTAC-7. The *Y* axis represents the RMSF values in molecular distance unit, i.e. Angstrom (Å) while the *X* axis indicates the specific position of the residue.

exhibited (–10.0 Kcal/mol) binding energy with main protease 6LU7. PHE291, GLN127, ARG4, and LYS5 are the amino acid residues participating in the interaction at the binding pocket of COVID-19 (Figure 6). The 2D schematic representation of protein–ligand interaction is represented by LIGPLOT representing the major amino acid residues of TAC-4 binding on the active site pocket of the protein 6LU7The molecular docking study in our study showed the inhibitory potential of 4 compounds, ranked by affinity (ΔG); TAC-6 > TAC-3 > TAC-4 > TAC-7.

3.1. ADME calculations

Next, to get an insight about the drug-likeness properties of the lead compounds, all the 14 compounds were screened for ADME properties using swiss ADME programme and the results are shown in Table 3. The major criteria to understand the drug likeness properties of a particular compound involves Lipinski's rule of five (ROF) and if a specific lead compound with a certain pharmacological and biological activity has chemical and physical properties would make it a likely orally active drug in humans. Lipinski's rule of five suggests the molecular properties which are critical in order to understand the drug's pharmacokinetics in the human body for example absorption, distribution, metabolism, and excretion (ADME).

An ideal drug following Lipinski's rule of five criteria are (i) molecular mass of a compound less than 500 Daltons, (ii) no more than 5 hydrogen bond donors, (iii) no more than 10 hydrogen bond acceptors, (iv) an octanol-water partition coefficient log P not greater than 5. Three or more than 3 violations of the Lipinski's rule do not fit into the criteria of drug likeliness and ideally it is not generally considered for further drug discovery. However, it is very important to

mention that Lipinski's rule of five is not applicable to certain class of natural products and drugs which are substrates of biological transporters such as antibodies and proteins and antibodies and are successfully FDA approved and widely distributed in the market. Although in our study, all the four triarylchromones (TAC 3, 4, 6 and 7) are not following Lipinski's rule of five. However, the selected compounds docked against main protease 6LU7 have been validated using molecular dynamics simulation studies and the results revealed that the selected lead compounds were identified as the most suitable target against SARS-CoV-2 main protease 6LU7. Therefore, this preliminary screening process of potential compounds would facilitate in providing the fast *in silico* analysis towards development of therapeutic agent against SARS-CoV-2 (COVID-19).

3.2. Molecular dynamics (MD) simulation

All four complexes (complex TAC-3, TAC-4, TAC-6, and TAC-7) were simulated for 100 ns and the final structure exhibited good stereochemical geometry of the residues as analyzed by Ramachandran map (Figure 7A–D). The proteins in all four complexes were stabled with only 1–3 residues in outlier region. Both complex TAC-3 and complex TAC-7 have only one residue (Asp33) in outlier region while complex TAC-4 and complex TAC-6 have 3 (Asp33, Asn84, Tyr154) and 2 (Asp33, Asn84), respectively. It was found that Asp33 is the most common residue lie in outlier region in all four complexes. These number of residues in favoured, additional allowed, generously allowed and outlier region along with their percentage given in Table 4.

The Ramachandran plot showed good steriochemical geometry of residues of protein for all four complexes
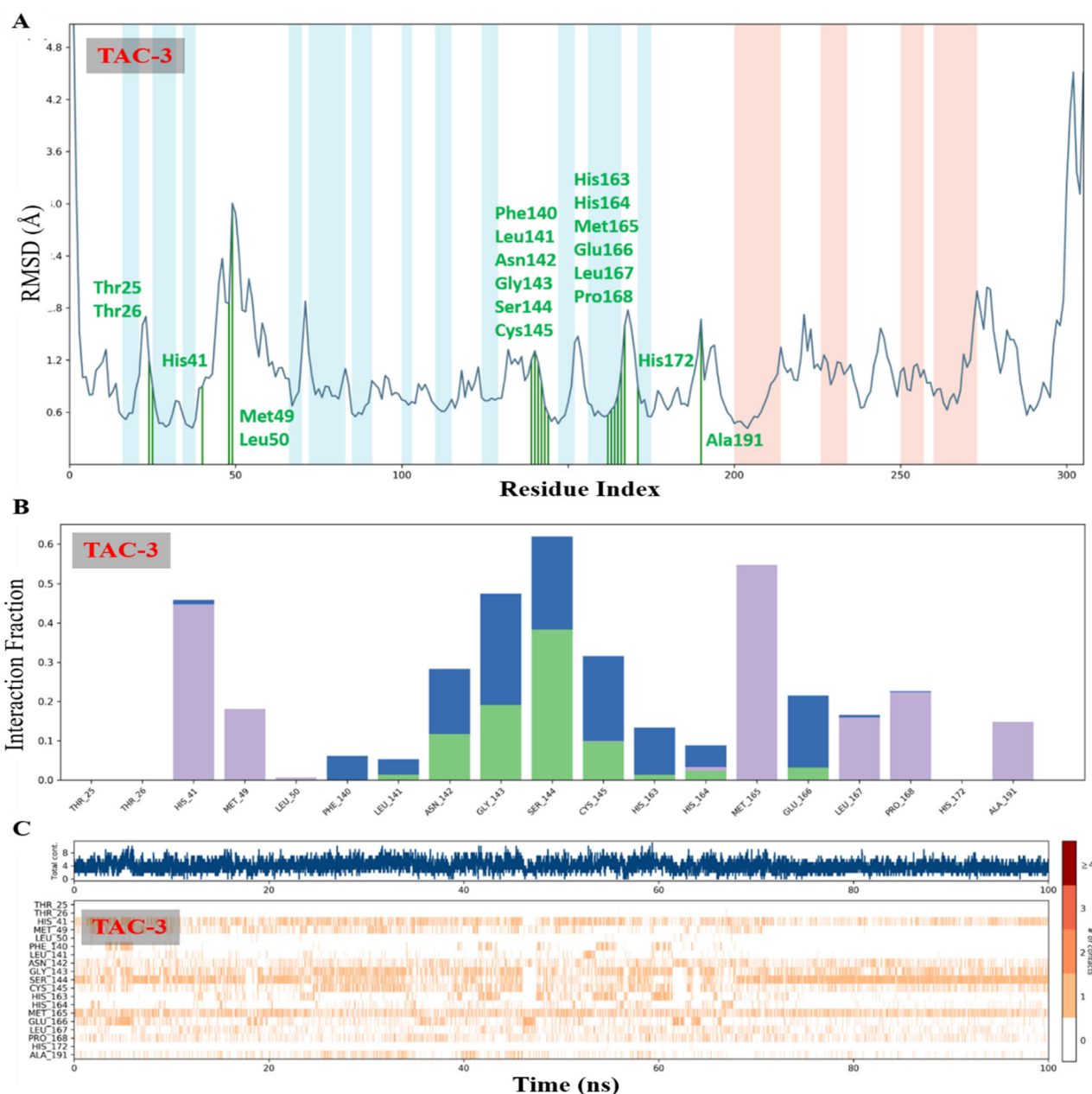
Figure 11. Complex TAC-3: (A) RMSF plot of residue number and C-alpha of spike protein at 100 ns simulation. It predicts the fluctuations of the C-alpha atoms; residues are shown in three letter code with their respective number in green colour belong to binding site residues interacting to compound shown in green line. (B) The histogram of protein–ligand contact over the course of the trajectory (C) A timeline representation of the interactions and contacts (H-bonds, hydrophobic, ionic, water bridges) with compound. The top panel shows the total number of specific contacts the protein–ligand complex in each trajectory frame. The bottom panel shows binding site residues interact with the ligand in each trajectory frame.

complex. The binding free energy for these four docked complexes were also calculated by MMGBSA as given in Table 5 where compound in complex TAC-3 has lowest binding free energy of −78 kcal/mol among all compounds. This generalized Born model and solvent accessibility method of force field optimization to elicit free energies from structural information circumventing the computational complexity of free energy simulations. Molecular dynamics simulation study of all four complexes for 100 ns was done to analyze the stability of docked ligand within the binding pocket where ligand interacted with active domain of proteins through water bridges, hydrophobic interactions, salt bridge and H-bonds. The Cα RMSD is not deviated so much in all four complexes (Figure 8).

It suggests the structural stability of protein in all four complexes but ligand RMSD plot showed least deviation in ligand in complex TAC-3 as compare to other three complex TAC-4, 6, and 7 (Figure 9A–D). Ligand RMSD indicates how stable the ligand is with respect to the protein and its binding pocket. The plot (Figure 9A–D) show the RMSD of a ligand when the protein–ligand complex is first aligned on the protein backbone of the reference and then the RMSD of the ligand is measured. The similarly, ligand root mean square fluctuation (RMSF) is also least fluctuating for ligand within complex TAC-3 among all complexes (Figure 10A–D). It indicates conformational stability of compound in complex TAC-3. The RMSF is useful for characterizing local changes along
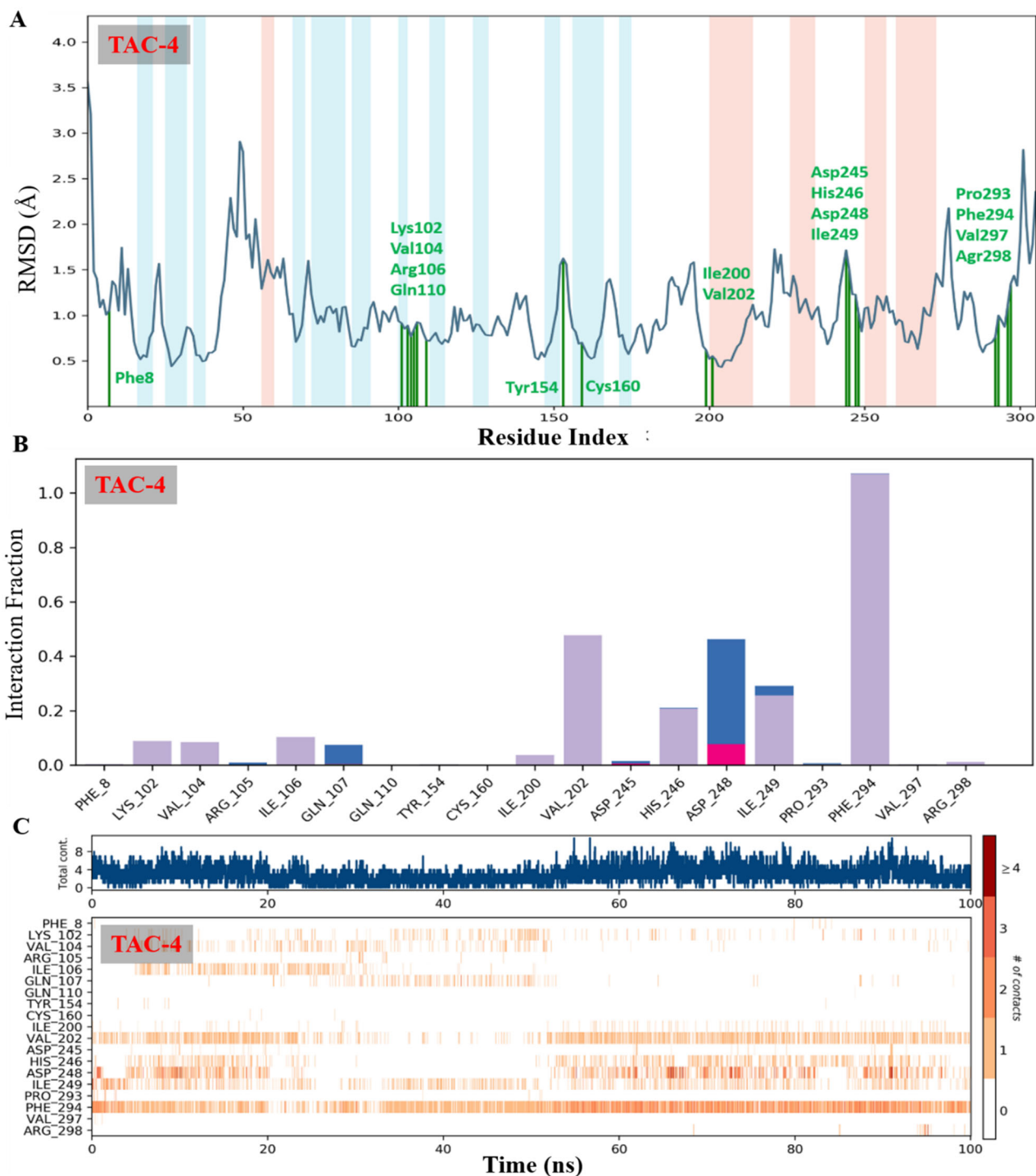
Figure 12. ComplexTAC-4: (A) RMSF plot of residue number and C-alpha of spike protein at 100 ns simulation. It predicts the fluctuations of the C-alpha atoms; residues are shown in three letter code with their respective number in green colour belong to binding site residues interacting to compound shown in green line. (B) The histogram of protein–ligand contact over the course of the trajectory (C) A timeline representation of the interactions and contacts (salt bridge, hydrophobic, ionic, water bridges) with compound. The top panel shows the total number of specific contacts the protein–ligand complex in each trajectory frame. The bottom panel shows binding site residues interact with the ligand in each trajectory frame.

the protein chain. TAC-3 showed less fluctuations than others, indicates that the ligand is stable in TAC-3 complex along the protein chain during simulation. The molecular dynamic study strongly validated the molecular docking data of protein ligand interaction for complex TAC-3 as compare to other complexes. It is very clear after trajectory analysis that ligand in complex TAC-3 is very stable than others. Figure 11A shows protein RMSF of ligand–protein complex

interacting with binding site residues of protein where Thr25, Thr26, His41, Met49, Leu50, Phe140, Leu141, Asn142, Gly143, Ser144, Cys145, His163, His164, Met165, Glu166, Leu167, Pro168, His172, and Ala191residues are interacting to compound where all binding site residues have RMSF <2Å except Leu50 shown by green lines matching the residue index, while the pink and blue bands indicate protein secondary structures helices and β-strands, respectively.
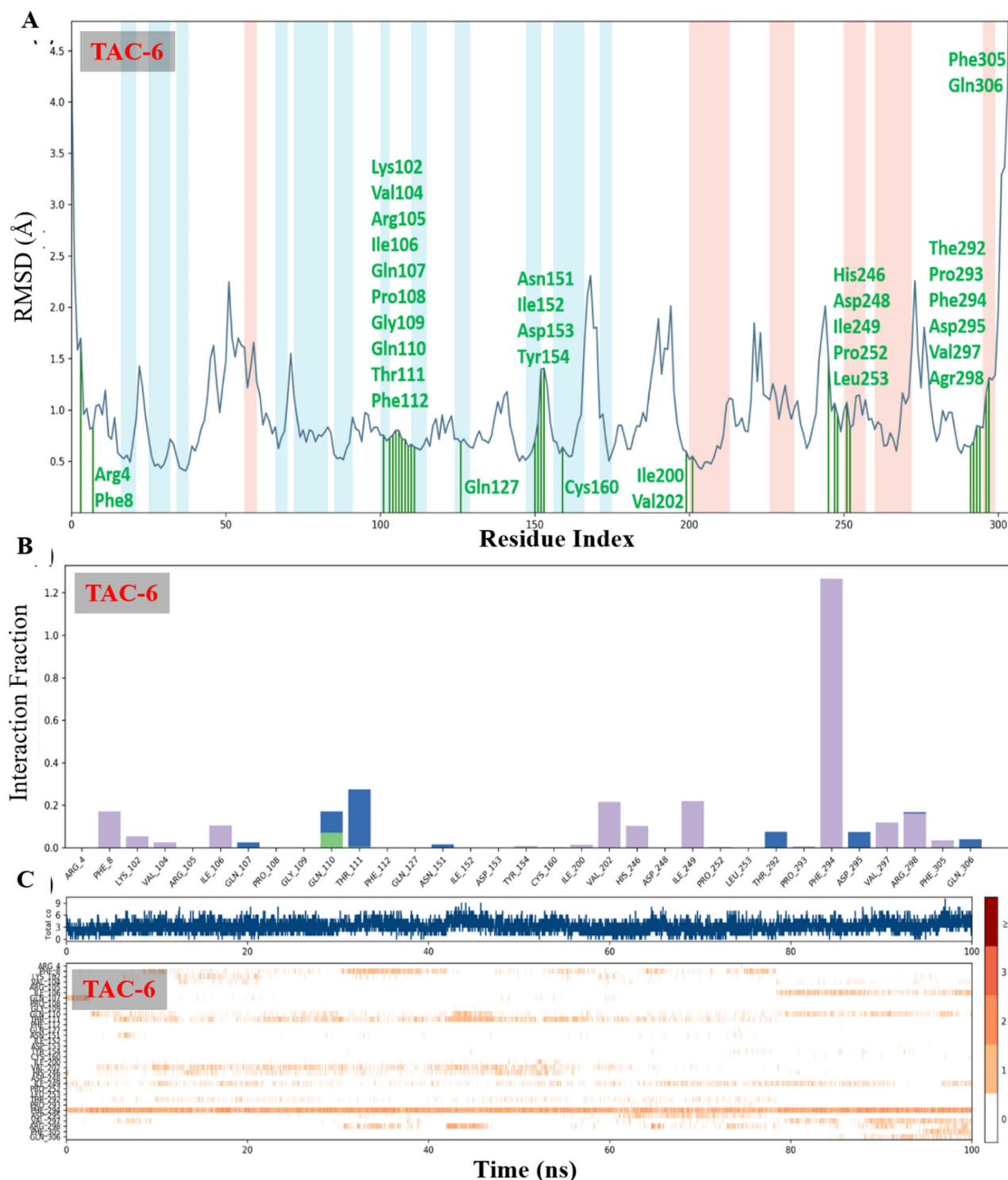
Figure 13. Complex TAC-6: (A) RMSF plot of residue number and C-alpha of spike protein at 100 ns simulation. It predicts the fluctuations of the C-alpha atoms; residues are shown in three letter code with their respective number in green colour belong to binding site residues interacting to compound shown in green line. (B) The histogram of protein–ligand contact over the course of the trajectory (C) A timeline representation of the interactions and contacts (salt bridge, hydrophobic, ionic, water bridges) with compound. The top panel shows the total number of specific contacts the protein–ligand complex in each trajectory frame. The bottom panel shows binding site residues interact with the ligand in each trajectory frame.

The type of interaction between compound and protein can be seen in Figure 11B where 3 kinds of interaction between ligand and protein such as H-bond (green), water bridge (blue), and hydrophobic interaction (grey) can be seen. There was no ionic interaction in complex. The bottom panel of Figure 11C shows the total number of contacts, the protein makes with the ligand over the course of the trajectory. While the bottom

panel shows which residues interact with the ligand in each trajectory frame. Some residues make more than one specific contact with the ligand, which is represented by a darker shade of orange, according to the scale to the right of the plot. Even binding free energy after MD simulation was further calculated and found that ligand in TAC-3 has lowest binding energy over others (Table 4). Moreover, TAC-4 (Figure 12A–C), TAC-6
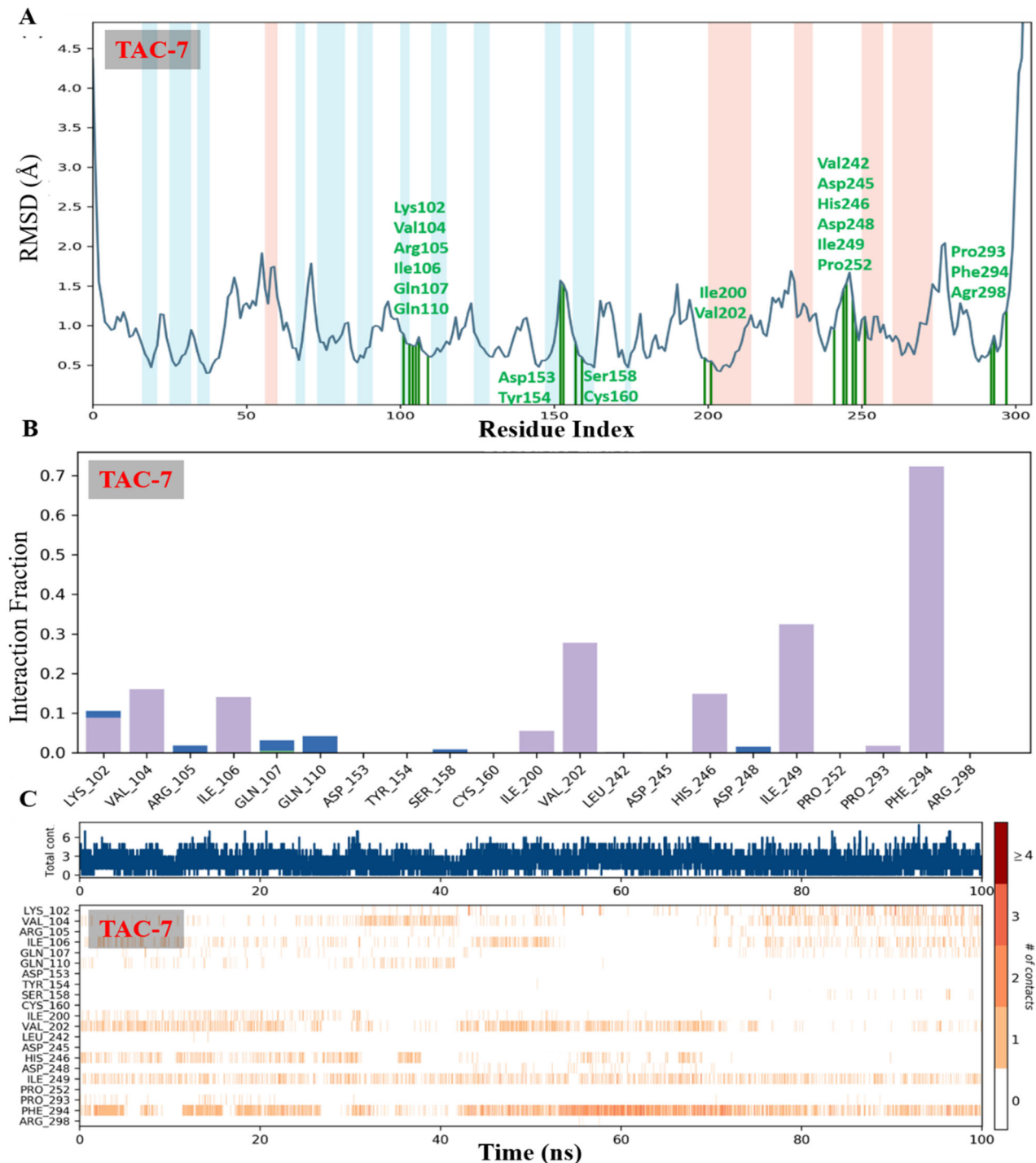
Figure 14. ComplexTAC-7: (A) RMSF plot of residue number and C-alpha of spike protein at 100 ns simulation. It predicts the fluctuations of the C-alpha atoms; residues are shown in three letter code with their respective number in green colour belong to binding site residues interacting to compound shown in green line. (B) The histogram of protein–ligand contact over the course of the trajectory (C) A timeline representation of the interactions and contacts (hydrophobic, water bridges) with compound. The top panel shows the total number of specific contacts the protein–ligand complex in each trajectory frame. The bottom panel shows binding site residues interact with the ligand in each trajectory frame.

(Figure 13A–C) and TAC-7 (Figure 14A–C) also showed strong stability at the active site of the protein (main protease of SARS-CoV-2).

4. Conclusion

The identification of potent/effective molecules against infectious diseases including COVID-19 are always appreciable. As we already know by now, COVID-19 has hugely impacted the socio-economic status of the several countries across the world. In this situation, the identification of an effective and reliable drug molecule against COVID-19 targeting through main protease of SARS-CoV-2 will help us to develop potential therapeutic approach which could save millions of people globally. In this *in silico* study, we have identified triarylchromones (*TAC*) derivatives as potent inhibitors

against main protease of SARS-CoV-2 which can be further tested against the SARS-CoV-2 at *in vitro* and *in vivo* model for the development of therapeutic approach for COVID-19.

Acknowledgements

Disclosure statement

The authors declare no conflict of interest

References

Akaji, K., Konno, H. (2020). Design and evaluation of anti-SARS-coronavirus agents based on molecular interactions with the viral protease. *Molecules*, 25(17), 3920. https://doi.org/10.3390/molecules25173920

Ali, A., & Vijayan, R. (2020). Dynamics of the ACE2–SARS-CoV-2/SARS-CoV spike protein interface reveal unique mechanisms. *Science Reports*, 10, 14214. https://doi.org/10.1038/s41598-020-71188-3

Astuti, I., & Ysrafil (2020). Severe acute respiratory syndrome coronavirus 2 (SARS-CoV-2): An overview of viral structure and host response. *Diabetes & Metabolic Syndrome*, 14(4), 407–412. https://doi.org/10.1016/j.dsx.2020.04.020

Aucoin, M., & Cooley, K. (2020). The effect of quercetin on the prevention or treatment of COVID-19 and other respiratory tract infections in humans: A rapid review. *Advanced & Integrated Medicine*, 7(4), 247–251. https://doi.org/10.1016/j.aimed.2020.07.007

Cao, B., & Yang. Y. (2020). A trial of lopinavir–ritonavir in adults hospitalized with severe Covid-19. *New England Journal of Medicine*, 382, 1787–1799. https://doi.org/10.1056/NEJMoa2001282

Chaccour, C., Abizanda, G., Irigoyen-Barrio, Á., et al. (2020). Nebulized ivermectin for COVID-19 and other respiratory diseases, a proof of concept, dose-ranging study in rats. *Scientific Reports*, 10, 17073. https://doi.org/10.1038/s41598-020-74084-y

Chandel, V., Raj, S., Rathi, B., & Kumar, D. (2020). *In silico* identification of potent FDA approved drugs against coronavirus covid-19 main protease: A drug repurposing approach. *Chemical Biology Letters*, 7(3), 166–175.

Chandel, V., Srivastava, M., Srivastava, A., Asthana, S., & Kumar, D. (2020). *In-silico* interactions of active phytochemicals with c-Myc EGFR and ERBB2 oncoproteins. *Chemical Biology Letters*, 7(1), 47–54.

Choi, H., Min, M., et al. (2016). Unraveling innate substrate control in site-selective palladium-catalyzed C–H heterocycle functionalization. *Chemical Sciences*, 7, 3900–3909. https://doi.org/10.1039/c5sc04590h

Coelho, C., Gallo, G., Campos, C. B., Hardy, L., & WüRtele, M. (2020). *PLoS One*, 15(10), e0240079. https://doi.org/10.1371/journal.pone.0240079

Daina, A., & Michielin O., & Vincent, Z. (2007) SwissADME: A free web tool to evaluate pharmacokinetics, drug-likeness and medicinal chemistry friendliness of small molecules. *Scientific Reports*, 7, 1–13. https://doi.org/10.1038/srep42717

Derosa, G., Maffioli, P., D'Angelo, A., & Di Pieero, F. (2020). Drugs against coronavirus COVID-19 main protease: A drug repurposing approach. *Chemical Phytotherapy & Research*, 35,1230–1236. https://doi.org/10.1002/ptr.6887

Ferner, R. E., & Aronson, J. K. (2020). Chloroquine and hydroxychloroquine in covid-19. *British Medical Journal*, 369, m1432. https://doi.org/10.1136/bmj.m1432

Focosi, D., Anderson, A. O., Tang, J. W., & Tuccori, M. (2020). Convalescent plasma therapy for COVID-19: State of the art. *Clinical Microbiology & Review*, 33(4), e00072-20. https://doi.org/10.1128/CMR.00072-20

Gaspar, A., Matos, M. J., Garrido, J., Uriarte, E., & Borges, F. (2014). Chromone: A valid scaffold in medicinal chemistry. *Chemical Review*, 114(9), 4960–4992. https://doi.org/10.1021/cr400265z

Gavriatopoulou, M., Korompoki, E., Fotiou, D., Ntanasis-Stathopoulos, I., Psaltopoulou, T., Kastritis, E., Terpos, E., & Dimopoulos, M. A. (2020) Organ-specific manifestations of COVID-19 infection. *Clinical & Experimental Medicine*, 20(4), 493–506. https://doi.org/10.1007/s10238-020-00648-x

Guy, R. K., DiPaola, R. S., Romanelli, F., & Dutch, R. E. (2020). Rapid repurposing of drugs for COVID-19. *Science*, 368(6493), 829–830. https://doi.org/10.1126/science.abb9332

Harrison, C. (2020). Coronavirus puts drug repurposing on the fast track. *Nature Biotechnology*, 38(4), 379–381. https://doi.org/10.1038/d41587-020-00003-1

https://covid19.who.int/. (2020)

https://www.nature.com/articles/d41586-020-03248-7. (2020)

https://www.pfizer.com/news/press-release/press-release-detail/pfizer-and-biontech-announce-vaccine-candidate-against. (2020)

Huang, Chaolin, Wang, Yeming, Li, Xingwang, Ren, Lili, Zhao, Jianping, Hu, Yi, Zhang, Li, Fan, Guohui, Xu, Jiuyang, Gu, Xiaoying, Cheng, Zhenshun, Yu, Ting, Xia, Jiaan, Wei, Yuan, Wu, Wenjuan, Xie, Xuelei, Yin, Wen, Li, Hui, Liu, Min, Xiao, Yan, Gao, Hong, Cao, Bin, et al., (2020). Clinical features of patients infected with 2019 novel coronavirus in Wuhan, China, *Lancet*, 395(10223), 497–506. https://doi.org/10.1016/S0140-6736(20)30183-5

Huang, Y., Yang, C., Xu, X. F., et al. (2020). Structural and functional properties of SARS-CoV-2 spike protein: Potential antivirus drug development for COVID-19. *Acta Pharmacology Sinica*, 41, 1141–1149. https://doi.org/10.1038/s41401-020-0485-4

Jackson, L. A., Anderson, E. J., et al. (2020). An mRNA vaccine against SARS-CoV-2 – Preliminary report. *New England Journal of Medicine*, 383,1920–193. https://doi.org/10.1056/NEJMoa2022483

Keri, R. S., Budagumpi, S., Pai, R. K., & Balakrishna, R. G. (2014). *European Journal of Medicinal Chemistry*, 78, 340–374. https://doi.org/10.1016/j.ejmech.2014.03.047

Kim, K. H., Lee, H. S., Kim, S. H., & Kim, J. N. (2012). Palladium-catalyzed oxidative arylation of chromones via a double C–H activation: An expedient approach to flavones. *Tetrahedron Letters*, 53(22), 2761–2764. https://doi.org/10.1016/j.tetlet.2012.03.100

Krammer, F. (2020). SARS-CoV-2 vaccines in development. *Nature*, 586, 516–527. https://doi.org/10.1016/j.immuni.2020.03.007

Kumar, A., Singh, A. K., & Tripathi, G. (2020). Phytochemicals as potential curative agents against viral infection: A review. *Current Organic Chemistry*, 24(20), 2356–2366. https://doi.org/10.2174/1385272824999200910093524

Lammers, T., Sofias, A. M., van der Meel, R., et al. (2020). Dexamethasone nanomedicines for COVID-19. *Nature Nanotechnology*, 15, 622–624. https://doi.org/10.1038/s41565-020-0752-z

Morris, G., Huey, R., Lindstrom, W., et al. (2009). AutoDock4 and AutoDockTools4: Automated docking with selective receptor flexibility. *Journal of Computer Chemistry*, 30(16), 2785–2791. https://doi.org/10.1002/jcc.21256

Morris, M., Huey R., & Olson, A. J. (2008). Using Autodock for receptor ligand docking. *Current Protocols Bioinformatics*, 30(16), 2785–2791. https://doi.org/10.1002/0471250953.bi0814s24

Portelli, S., Olshansky, M., & Rodrigues, C. H. M., et al. (2020). Exploring the structural distribution of genetic variation in SARS-CoV-2 with the COVID-3D online resource. *Nature Genetics*, 52, 999–1001. https://doi.org/10.1038/s41588-020-0693-3

Preeti, P., Jitendra, S. R., Aroni, C., Abhijeet, K., Rajni, K., Amresh, P., & Shashikant, R. (2020). Targeting SARS-CoV-2 spike protein of COVID-19 with naturally occurring phytochemicals: An *in silico* study for drug development. *Journal of Biomolecular Structure & Dynamics*, 1–15. https://doi.org/10.1080/07391102.2020.1796811

Rane, J. S., Pandey, P., Chatterjee, A., Khan, R., Kumar, A., Prakash, A., & Ray, S. (2020). Targeting virus–host interaction by novel pyrimidine derivative: An *in silico* approach towards discovery of potential drug against COVID-19. *Journal of Biomolecular Structure & Dynamics*. https://doi.org/10.1080/07391102.2020.1794969

Rao, M. L. N., & Kumar, A. (2014). Pd-catalyzed atom-economic couplings of triarylbismuth reagents with 2-bromo- and 2,6-dibromochromones and synthesis of medicinally important fisetin. *Tetrahedron Letters*, 55(42), 5764–5770. https://doi.org/10.1002/ejoc.201201314

Rashmi, T., Mitul, S., Preeti, J., Ramendra, P. P., Shailendra, A, Dhruv, K., & Samuel, R. (2020). Development of potential proteasome inhibitors

against *Mycobacterium tuberculosis*. *Journal of Biomolecular Structure & Dynamics*, *19*, 1–15. https://doi.org/10.1080/07391102.2020.1835722

Rauf, M. A., Zubair, S., & Azhar, A. (2015). Ligand docking and binding site analysis with pymol and autodock/vina. *International Journal of Basic & Applied Sciences*, *4*(2), 168. https://doi.org/10.14419/ijbas.v4i2.4123

Reis, J., Gaspar, A., Milhazes, N., & Borges, F. (2017) Chromone as a privileged scaffold in drug discovery: Recent advances. *Journal of Medicinal Chemistry*, *60*, 7941–7957. https://doi.org/10.1021/acs.jmedchem.6b01720

Rohit, S., Niraj, K. J., Rohan, K., Saurabh, K. J., Ankur, S., Dhruv, K., et al. (2020) Deciphering the SSR incidences across viral members of Coronaviridae family. *Chemical Biology & Interaction*, *331*(109226). https://doi.org/10.1016/j.cbi.2020.109226

Schrödinger Release 2020-1: Maestro, Schrödinger, LLC, New York, NY, 2020.

Schrödinger Release 2020-1: Prime, Schrödinger, LLC, New York, NY, 2020.

Schrödinger Release 2020-1: Protein Preparation Wizard; Epik, Schrödinger, LLC, New York, NY, 2016; Impact, Schrödinger, LLC, New York, NY, 2016; Prime, Schrödinger, LLC, New York, NY, 2020

Serafin, M. B., Bottega, A., Foletto, V. S., da Rosa, T. F, Hörner. A., & Hörner, R. (2020). Drug repositioning is an alternative for the treatment of coronavirus COVID-19. *International Journal of Antimicrobial Agents*, *55*(6), 105969. https://doi.org/10.1016/j.ijantimicag.2020.105969

Seri, J., Suwon, K., Dae Y.K., Mi-Sun, K., & Dong H. S. (2020) Flavonoids with inhibitory activity against SARS-CoV-2 3CLpro. *Journal of Enzyme Inhibitors & Medicinal Chemistry*, *35*(1), 1539–1544. https://doi.org/10.1080/14756366.2020.1801672

Straughn, A. R., & Kakar, S. S. (2020). Withaferin A: A potential therapeutic agent against COVID-19 infection. *Journal of Ovarian Research*, *13*, 79. https://doi.org/10.1186/s13048-020-00684-x

Sumit, K., Prem, P. S., Uma, S., Dhruv, K., et al. (2020) Discovery of new hydroxyethylamine analogs against 3CLpro protein target of SARS-CoV-2: Molecular docking, molecular dynamics simulation, and structure–activity relationship studies. *Journal of Chemistry & Information Model.* *60*(12), 5754–5770. https://doi.org/10.1021/acs.jcim.0c00326

Tregoning, J. S., Brown, E. S., Cheeseman, H. M., et al. (2020) Vaccines for COVID-19. *Clinical & Experimental Immunology*, *202*(2), 162–192. https://doi.org/10.1111/cei.13517

V'kovski, P., Kratzel, A., Steiner, S., et al. (2020) Coronavirus biology and replication: Implications for SARS-CoV-2. *Nature Review of Microbiology*, *19*, 155–170. https://doi.org/10.1038/s41579-020-00468-6

Vaishali, C., Prem Prakash, S., Sibi, R., Ramesh, C., Rathi, B., & Kumar, D. (2020). Structure-based drug repurposing for targeting Nsp9 replicase and spike proteins of severe acute respiratory syndrome coronavirus 2. *Journal of Biomolecular Structure & Dynamics*, *24*, 1–14. https://doi.org/10.1080/07391102.2020.1811773

Verma, S., Twilley, D., Esmear, T., Oosthuizen, C. B., Reid, A.-M., Nel, M., & Lall, N. (2020) Anti-SARS-CoV natural products with the potential to inhibit SARS-CoV-2 (COVID-19). *Frontiers in Pharmacology*, *11*, 561334. https://doi.org/10.3389/fphar.2020.561334

Vincet, J-L., & Taccone, F. S. (2020). Understanding pathways to death in patients with COVID-19. *Lancet*, *8*(5), 430–432. https://doi.org/10.1016/S2213-2600(20)30165-X

Vivek, P., Garima, T., Dhruv, K., Abhijeet, K., & Pawan, K.D. (2020). Novel 3,4-diarylpyrazole as prospective anti-cancerous agents. *Heliyon*, *6*(7), e04397. https://doi.org/10.1016/j.heliyon.2020.e04397

Walsh, E. E., Frenck, R. W., et al. (2020). Safety and immunogenicity of two RNA-based COVID-19 vaccine candidates. *New England Journal of Medicine.* *383*, 2439–2450. https://doi.org/10.1056/NEJMoa2027906

Wang, Y., Zhang, D., et al. (2020). Remdesivir in adults with severe COVID-19: A randomised, double-blind, placebo-controlled, multi-centre trial. *Lancet*, *395*, 1569–78. https://doi.org/10.1016/S0140-6736(20)31022-9

Wu, C., Liu, Y., Yang, Y., Zhang, P., Zhong, W., Wang, Y., Wang, Q., Xu, Y., Li, M., Li, X., Zheng, M., Chen, L., & Li, H. (2020). Analysis of therapeutic targets for SARS-CoV-2 and discovery of potential drugs by computational methods. *Acta Pharmaceutica Sinica B*, *10*(5), 766–788. https://doi.org/10.1016/j.apsb.2020.02.008

Yang, Y., Xiao, Z., Ye, K., et al. (2020) SARS-CoV-2: Characteristics and current advances in research. *Virology Journal*, *17*, 117. https://doi.org/10.1186/s12985-020-01369-z

Zhang, L., Lin, D., Sun, X., Curth, U., Drosten, C., Sauerhering, L., Becker, S., Rox, K., & Hilgenfeld, R. (2020). Crystal structure of SARS-CoV-2 main protease provides a basis for design of improved α-ketoamide inhibitors. *Science*, *368*(6489), 409–412. https://doi.org/10.1126/science.abb3405

Zhao, C., Qin, G., Niu, J., Wang, Z., Wang, C., Ren, J., & Qu, X. (2021). Targeting RNA G-quadruplex in SARS-CoV-2: A promising therapeutic target for COVID-19? *Angewandte Chemie International Edition*, *60*(1), 432–439. https://doi.org/10.1002/anie.202011419

Zheng, J. (2020) SARS-CoV-2: An emerging coronavirus that causes a global threat. *International Journal of Biological Science*, *16*(10), 1678–1685. https://doi.org/10.7150/ijbs.45053

Zhu, N., Zhang, D., Wang W., et al. (2020). A novel coronavirus from patients with pneumonia in China, 2019. *New England Journal of Medicine*, *382*, 727–733. https://doi.org/10.1056/NEJMoa2001017

Zhu, W., Xu, M., Chen, C. Z, Guo, H., Shen, M., Hu, X., Shinn, P., Klumpp-Thomas, C., Michael S. G., & Zheng, W. (2020) Identification of SARS-CoV-2 3CL protease inhibitors by a quantitative high-throughput screening. *ACS Pharmacology & Translational Science*, *3*(5), 1008–1016. https://doi.org/10.1101/2020.07.17.207019